International Journal of Engineering and Geosciences
https://dergipark.org.tr/en/pub/ijeg
e-ISSN 2548-0960

A comparative spectral assessment approach of SEBAL and SEBS for actual evaporation estimation in Ardabil Province

Khalil Valizadeh Kamran [*1], **Mahmoud Sourghali** [1], **Samaneh Bagheri** [1]

[1] *University of Tabriz, Department of Remote Sensing and GIS, Iran, valizadeh@tabrizu.ac.ir, m.soorghali@gmail.com, samanehbagheri99@gmail.com*

Cite this study: Valizadeh Kamran, K., Sourghali, M., & Bagheri, S. (2024). A comparative spectral assessment approach of SEBAL and SEBS for actual evaporation estimation in Ardabil Province. International Journal of Engineering and Geosciences, 9 (2), 131-146

https://doi.org/10.26833/ijeg.1344679

Keywords
Evapotranspiration
Mughan plain
OLI and TIRS sensors
SEBAL
SEBS

Research Article

Received: 17.08.2023
Revised: 03.12.2023
Accepted: 09.12.2023
Published:23.07.2024

Abstract

Evapotranspiration is a crucial process in the Earth's water and climate cycle, responsible for transforming water from liquid to water vapor. This transformation plays a vital role in the global water cycle and has a significant impact on the climate, weather patterns, and precipitation in various regions. In this study, actual evapotranspiration in the Mughan plain of Ardabil province has been estimated using spectral data from the OLI and TIRS sensors of the Landsat 8 satellite. The SEBAL (Surface Energy Balance Algorithm for Land) and SEBS (Surface Energy Balance System) methods have been employed to calculate these phenomena. SEBAL is an energy balance algorithm designed for land surfaces, utilizing satellite data to estimate actual evapotranspiration accurately. Similarly, SEBS is a surface energy balance system that provides a more precise estimation of evapotranspiration and transpiration rates. Data from the OLI and TIRS sensors of Landsat 8 were collected from the study area for this research. By applying the SEBAL and SEBS methods to these data, actual evapotranspiration values in the Mughan plain were obtained. The results indicated that SEBAL showed a broader range of actual evapotranspiration values (0.74 to 5.8 mm) compared to SEBS (1.25 to 8.85 mm), highlighting its ability to distinguish different regions with varying evapotranspiration rates. However, SEBAL's implementation is more computationally demanding than SEBS, making the calculation process time-consuming. Overall, both algorithms demonstrated relatively high capabilities in calculating instantaneous evapotranspiration using spectral data. The findings of this study can be valuable for water resources and agricultural management in the research area, as well as for water resource planning and environmental studies.

1. Introduction

In recent years, with the development of remote sensing technologies, many mapping techniques and analyzes have been developed [1]. Remote sensing has long been an important and effective tool for monitoring land cover, with its ability to quickly provide broad, precise, unbiased and easily accessible information regarding the spatial variability of the land surface.

Problems such as global warming and climate change have increased their negative impact in the world in recent years [2]. On the one hand, the use of water resources has been limited, and on the other hand, water consumption in the agricultural sector has increased. while water consumption in the agricultural sector has increased. On the other hand, changes in land use and land cover are also influential factors [3]. Therefore, efficient use of available water resources, especially in agricultural uses, which constitute a significant portion of a country's water consumption, is essential. The agricultural sector consumes the largest volume of freshwater in the world, making an efficient method for managing freshwater resources crucial in each country. In this regard, the first step is to calculate the water requirements of plants. Evapotranspiration is a good indicator for assessing irrigation efficiency and overall water consumption of plants. Land surface evapotranspiration (ET) is of prime interest for environmental applications, such as optimizing irrigation water use, irrigation system performance, crop water deficit, drought mitigation strategies, and accurate initialization of climate prediction models especially in arid and semiarid catchments where water shortage is a critical problem [4].

Evaporation is a process through which water from the Earth's surface and water bodies returns to the atmosphere. This process involves the transfer of energy, where water molecules acquire 600 calories of heat, reach the state of vaporization, and are consequently released into the air. The amount of evaporation is influenced by various factors, including solar radiation, air dryness, water temperature, water concentration and color, wind speed, surface type, absolute humidity of the air, and atmospheric pressure.

Evapotranspiration potential, or simply potential evapotranspiration, refers to the amount of evaporation and transpiration that would occur under conditions where sufficient moisture is available throughout the entire period, or in other words, the water level that would be evaporated if moisture resources were present. On the other hand, actual evapotranspiration is the amount that occurs under the natural conditions of a specific region, and its value increases with more available water. However, the actual evapotranspiration will never exceed the potential evapotranspiration.

Asadi and Valizadeh Kamran [5] conducted a study comparing the algorithms SEBAL, METRIC, and ALARM for estimating actual evapotranspiration of wheat crops in the Parsabad-Moghan region in northwest Iran, which is one of the main agricultural areas in the country. The research utilized the Surface Energy Balance Algorithm for Land (SEBAL), Mapping Evapotranspiration at High Resolution with Internal Calibration (METRIC), and Analytical Land-Atmosphere Radiative Transfer Model (ALARM) as the research tools. Twelve satellite images from Landsat 7 and 8 were used, covering the crop development period from 2016 to 2019, and the results were compared with lysimeter data.

Yang et al. [6] conducted a study to estimate evapotranspiration (ET) by combining Bayesian Model Averaging (BMA) with machine learning algorithms. The objective of this study was to reduce errors and uncertainties among multiple ET models to improve daily ET estimation. The results indicated that the BMA method outperformed the eight individual models. Four significant models obtained through the BMA method were ranked based on Random Forest, SVM, SEBS, and SEBAL. The combination of BMA with machine learning can significantly improve the accuracy of daily ET estimation, reduce uncertainties among models, and leverage the distinct advantages of empirical and physical-based models to obtain more reliable ET estimates.

Wei et al. [7] conducted a study on rice growth stage identification and evapotranspiration (ET) estimation in paddy fields using an improved SEBAL model with the consideration of the practical application of the surface resistance equation. Comparison between the estimation results and covariance data showed that SEBALR can provide more accurate ET estimates compared to the original surface energy balance algorithm for land, with a root mean square error (RMSE) of 1.02 mm·d-1, mean relative error (MRE) of 22.97%, and Pearson correlation (R^2) of 0.790.

Ma et al. [8] conducted a study on estimating regional actual evapotranspiration (ET) using an improved SEBAL model. In this study, a Surface Energy Balance model based on SEBAL and improved sensible heat flux computations (Y-SEBAL) was proposed and used for simulating actual ET at a large scale.The results showed that the Y-SEBAL model's simulation performance was highly consistent with covariance measurement data, with an R value of 0.82, agreement index of 0.90, and root mean square error of 0.81 mm/d. The performance validation indices were better than those of the SEBAL, MOD16, and SSEBop models. The Y-SEBAL model demonstrated the highest sensitivity to wind speed, reaching 0.714.

Therefore, our goal of this research is to estimate plant water needs and optimal management of water resources. For this purpose, SEBAL and SEBS spectra were compared to estimate actual evaporation and transpiration in the study area and the efficiency of these two algorithms was compared. In this regard, we continued to introduce these two algorithms, using each of these two algorithms, we calculated the rate of evaporation and transpiration and compared their results.

2. Material, methods and case studies

In this study, in order to estimate real evaporation and transpiration based on SEBAL and SEBS methods, we will use satellite images and meteorological data. The satellite image used is the spectral data of OLI and TIRS sensors of Landsat 8 satellite. Meteorological data was also prepared from Iran Meteorological Organization.

2.1. Case studies

The study area is located in the northwest of Iran, specifically in Ardabil province, between the cities of Parsabad and Bilasuvar (Moghan Plain), (Figure 1). The area has an average elevation of 100 meters above sea level. The dominant crop in the study area at the time of image acquisition and actual evapotranspiration estimation is wheat.

2.2. Material and dataset

The main data required for implementing the SEBAL (Surface Energy Balance Algorithm for Land) model are satellite images and weather data. Analysis of the climate data series collected can provide insights about the changes in climatic conditions in the region [9].

2.2.1. Satellite data

The used images must be cloud-free. In this research, the OLI sensor images from Landsat 8 satellite were utilized. The Digital Image used corresponds to the date of 04/04/2021, and the local time is approximately 11:00 AM. To calculate evapotranspiration, bands 1 to 7, and also band 10 (thermal band) were utilized.

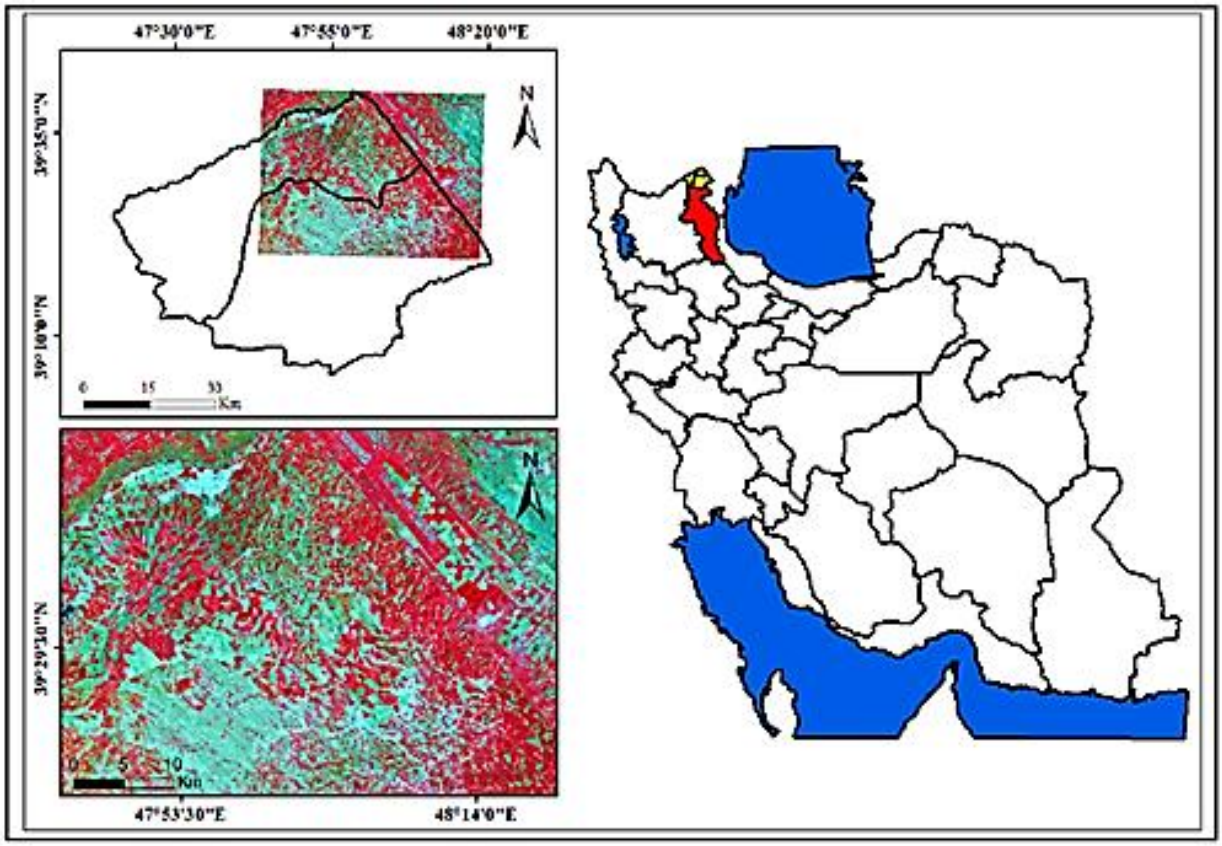

Figure 1. Study area.

2.2.2. Climate data

The climate data used in the model and for calculating the reference evapotranspiration (ETr) are presented in Table 1. In this research, data from two synoptic stations, Parsabad and Pileh Savar, were utilized, and the final values were obtained by averaging the corresponding measurements from these two stations. ETr represents the evapotranspiration of well-irrigated crops, which is used to calculate the sensible heat in the cold pixel area and ETrF. ETrF is similar to the crop coefficient (Kc), representing the ratio of instantaneous ET (ETinst) calculated for each pixel to the ETr calculated from climate data for the image time. ETrF is used for extrapolating ET from the image time to the 24-hour period (ET24) or longer. Its value ranges between zero and one ET24: Generally, daily ET values are more commonly used than instantaneous ET values. SEBAL calculates ET24 assuming that ETrF is constant over the 24-hour period (i.e., relatively constant throughout 24 hours). ET24 can be calculated (Equation 1) as follows [10]:

Table 1. Climate data used in the research.

Data used (unit)	value
Satellite overpass temperature (°C)	19
minimum daily temperature(°C)	6.5
Maximum daily temperature(°C)	21.5
Sunshine duration	10.7
Relative humidity (%)	37.5
Wind speed(M/S)	4
Station height(M)	100

$$ET_{24}=ET_rF\times ET_{r\text{-}24} \quad (1)$$

ET24: ET24 is the total accumulated evapotranspiration over a 24-hour period for the satellite passing day. It is calculated by summing up the hourly ETr values during the satellite passing day.

2.3. Methods

2.3.1. The SEBAL method

According to the definition, the total evaporation and transpiration from all surfaces of vegetation are referred to as evapotranspiration (ET). Regardless of the partial amount of water used in metabolic activities of plants, evapotranspiration can be considered as equivalent to the water consumed by the plant. Evapotranspiration is a process resulting from the turbulent transfer of energy. The complete energy balance equation can be expressed as Equation (2), where (Rn) represents the net incoming radiation to the surface, (G) is the soil heat flux, (H) is the sensible heat flux, and ETλ denotes the latent heat flux. In this equation, the term (Rn) corresponds to the net radiation received by the surface, while (G) and (H) represent the soil heat flux and sensible heat flux, respectively. Most plants use less than one percent of the received solar radiation during the day for photosynthesis. The heat storage in plants during the day is negligible, and thus, both photosynthesis and heat storage in plants can be disregarded in the energy balance equation. Satellite data provide continuous and temporally diverse information about spectral reflectance and surface radiation. To calculate surface heat fluxes (sensible and latent heat), a multi-stage energy balance algorithm based on physical principles

(SEBAL) has been designed. SEBAL uses surface temperature, surface reflectance, and the normalized difference vegetation index (NDVI) as inputs to estimate surface heat fluxes for various land surface covers. By relying on satellite data and a limited amount of meteorological data, the SEBAL model is capable of estimating evapotranspiration. This model calculates the net incoming radiation (Rn), soil heat flux (G), and sensible heat flux (H) (Equation 2), and then subtracts the soil heat flux and sensible heat from the net incoming radiation to obtain the remaining energy, which is equivalent to the energy used for evaporation and transpiration (ET), representing the energy spent on converting water from liquid to vapor (Equation 2 and 3).

$$Rn = G + H + \mathrm{ET}\lambda + \text{Heat storage in plants} + \text{Photosynthesis} \quad (2)$$

ETλ: Latent heat flux (W/m^2)
Rn: Net radiation (W/m^2)
G: Soil heat flux (W/m^2)
H: Sensible heat flux (W/m^2)

$$Rn = (1 - \alpha)\, Rs\downarrow + RL\uparrow - RL\downarrow - (1 - \varepsilon^{\circ})\, RL\downarrow \quad (3)$$

α: Surface albedo
RL↓: Incoming longwave radiation (W/m^2)
Rs↓: Incoming shortwave radiation (W/m^2)
↑ RL: Outgoing longwave radiation (W/m^2)
ε°: Broadband surface emissivity

2.3.1.1. Calculation of net radiation

Net radiation (Rn) at the surface is obtained by considering all incoming and outgoing radiation fluxes [10]. The value of net radiation should fall within the range of 100 to 700 W/m^2.

To generate the net radiation raster layer, the input parameters of surface albedo, outgoing longwave radiation, and incoming shortwave and longwave radiation were calculated as 0.895, 314.714, 6584.314, and 714.314 respectively. Raster layers of vegetation index, emissivity, and surface temperature were used as inputs to calculate the outgoing longwave radiation at the longwave band. Finally, the net incoming radiation (Rn) was computed.

2.3.1.2. Calculation of surface albedo (α):

Surface albedo is defined as the ratio of electromagnetic energy reflected from the soil and vegetation surface to the incoming energy at that surface.

To calculate surface albedo, satellite images were first loaded using the metadata file in ENVI 5.6 software. The Radiometric Calibration command was then used to calculate radiance and spectral reflectance for each band. Subsequently, αtoa (atmospherically-corrected albedo) was computed using the Equation 4 and 5:

$$\alpha toa = \sum(\omega\lambda \times \rho\lambda) \quad (4)$$

$$\omega\lambda = \frac{ESUN\lambda}{\Sigma ESUN\lambda} \quad (5)$$

αtoa: Atmospherically-corrected albedo
ρi: Spectral reflectance for each band
ωi: Weighting coefficient for each band
λi: Wavelength of the band
λmin and λmax: Minimum and maximum wavelengths, respectively

The weighting coefficients (ω) for each band of Landsat 8 are shown in Table 2.

Table 2. Weighting coefficients (ω) for each band of Landsat 8.

Band number	1	2	3	4	5	6	7
Weighting coefficients	0.19	0.2	0.2	0.17	0.11	0.09	0.008

Surface albedo is the ratio of the reflected solar radiation from the soil and vegetation surface to the incoming solar radiation [11]. Albedo is influenced by the surface characteristics such as vegetation, soil, and other cover types. The calculation of albedo is performed by correcting Equation (4) for atmospheric transparency effects (Equation 6).

$$\alpha = \frac{\alpha toa - \alpha path - radiance}{\tau sw2} \quad (6)$$

Γsw: Atmospheric transparency.
path_radianceα: Path radiance-induced albedo, with a value between 0.25 and 0.40. In the SEBAL model, a value of 0.30 is recommended [12], and in this study, a value of 0.30 was selected (Equation 7).

$$\Gamma sw = 0.75 + 2 \times 10\text{^-}5 \times Z \quad (7)$$

Z: Elevation above sea level in meters. This elevation should represent the elevation of the study area, and it is often recommended to use the elevation of the nearest weather station. In this study, an elevation of 100 meters was considered.

2.3.1.3. Calculation of incoming short wave radiation (Rs↓)

The shortwave incoming radiation (Rs↓) is the actual solar radiation that reaches the Earth's surface under clear atmospheric conditions. It can be calculated using Equation (8):

$$Rs\downarrow = Gsc \times Cos\theta \times dr \times \Gamma sw \quad (8)$$

Gsc: Solar constant (1367 W/m^2)
Cosθ: Cosine of the solar zenith angle
dr: Inverse square of the relative distance between the Earth and the Sun
Γsw: Solar radiation atmospheric transmission factor

The calculated values for dr and θ for the studied region are 0.96 and 23.772°, respectively.

2.3.1.4. Long wave output radiation (↑) RL

The outgoing longwave radiation (RL↑) is a type of thermal radiation with a wavelength longer than 8

micrometers that is emitted from the Earth's surface into the atmosphere. Its magnitude varies based on the spatial and temporal location and ranges between 200 to 700 watts per square meter.

Equation (9) can be used to calculate RL↑:

$$RL\uparrow = \varepsilon^{\circ} \times \sigma \times Ts\text{^}4 \quad (9)$$

ε°: Surface emissivity, which is the ratio of emitted thermal radiation to that of a perfect blackbody ($0 \leq \varepsilon^{\circ} \leq 1$)
σ: Stefan-Boltzmann constant (5.67×10^{-8} $W/m^2/K^4$)
Ts: Surface temperature in Kelvin

Please note that the value of RL↑ is influenced by the surface temperature and emissivity of the area at the time of imaging.

2.3.1.5. Long wave input radiation (RL ↓)

The input longwave radiation (RL↓) is the thermal radiation from the atmosphere towards the Earth's surface, measured in watts per square meter (W/m^2). It can be calculated using equation (11) and its value varies depending on the spatial and temporal location of the imaging, typically ranging between 200 to 500 W/m^2.

Equation (10) describes the calculation of RL↓:

$$RL\downarrow = \varepsilon a \times \sigma \times Ta\text{^}4 \quad (10)$$

where:
εa: Atmospheric emissivity, which is the ratio of emitted thermal radiation from the atmosphere to that of a perfect blackbody ($0 \leq \varepsilon a \leq 1$)
σ: Stefan-Boltzmann constant (5.67×10^{-8} $W/m^2/K^4$)
Ta: Air temperature near the surface in Kelvin

Please note that the value of RL↓ depends on the atmospheric emissivity and the air temperature near the Earth's surface at the time of imaging.

2.3.1.6. Vegetation indicators

The SEBAL (Surface Energy Balance Algorithm for Land) model accepts vegetation indices as input data to calculate surface emissivity, surface temperature, and outgoing longwave radiation in the energy balance equation. Therefore, two important vegetation indices used in this model are presented below:

2.3.1.6.1. Normalized difference vegetation index (NDVI)

NDVI is a vegetation index that is sensitive to vegetation cover but cannot eliminate the effects of background soil. Its values range between 1+ to 1- where positive values indicate healthy vegetation. NDVI is calculated using the following formula, by placing near-infrared (NIR) and red bands in the Equation 11 and executing it (Figure 2):

$$NDVI = (NIR - R) / (NIR + R) \quad (11)$$

2.3.1.6.2. Leaf area index (LAI):

LAI is a vegetation index that represents the ratio of the area covered by the vegetation canopy to the ground area beneath it. It is commonly calculated using the relationship between LAI and NDVI (Equation 12):

$$LAI = 4.04 * Ln(NDVI) + 7.04 \quad (12)$$

In this study, after performing radiometric and atmospheric corrections on the input imagery, the vegetation indices NDVI and LAI were generated (Figure 3).

2.3.1.7. Surface temperature

In order to generate the surface temperature layer, thermal band number 10 of Landsat 8 was utilized. After performing radiometric and atmospheric corrections on band 10, radiance and brightness temperature were calculated using Equations 13 and 14, respectively.

$$\text{Radiance } (\text{ʎ}) = 0.0370588^* (DN) + 3.2 \quad (13)$$

$$\text{Brightness Temperature } (Tb) = (K2/(\ln (K1 / \text{ʎ} + 1)) \quad (14)$$

K1: 774.89
K2: 1321.08

Subsequently, surface emissivity was calculated and corrected using Equation 15, and finally, surface temperature in Kelvin was computed using Equation 16.

$$\text{Ɛ (Emissivity)} = 1.009 + 0.047^* \ln (NDVI) \quad (15)$$

$$\text{Surface Temperature } (Ts) = Tb/1 + (\text{ʎ}^*Tb/\text{ɣ}) * \ln \text{Ɛ} \quad (16)$$

Tb: Brightness temperature
ʎ: Radiance
ɣ: 14380
Ɛ: Corrected emissivity

These calculations were performed to derive the surface temperature layer in Kelvin using the available thermal band data from Landsat 8 after radiometric and atmospheric corrections (Figure 4).

2.3.1.8. Surface emissivity

Surface emissivity is the ratio of the thermal radiation emitted by the Earth's surface to that emitted by a blackbody at a specific temperature. In the SEBAL model, two emissivity are defined: the narrowband emissivity (εNB) that represents the behavior of surface emission in the narrow thermal band (with a small bandwidth), and the broad emissivity (ε_0) that represents the behavior of surface emission in the broad thermal band (ranging from 6 to 14 micrometers).

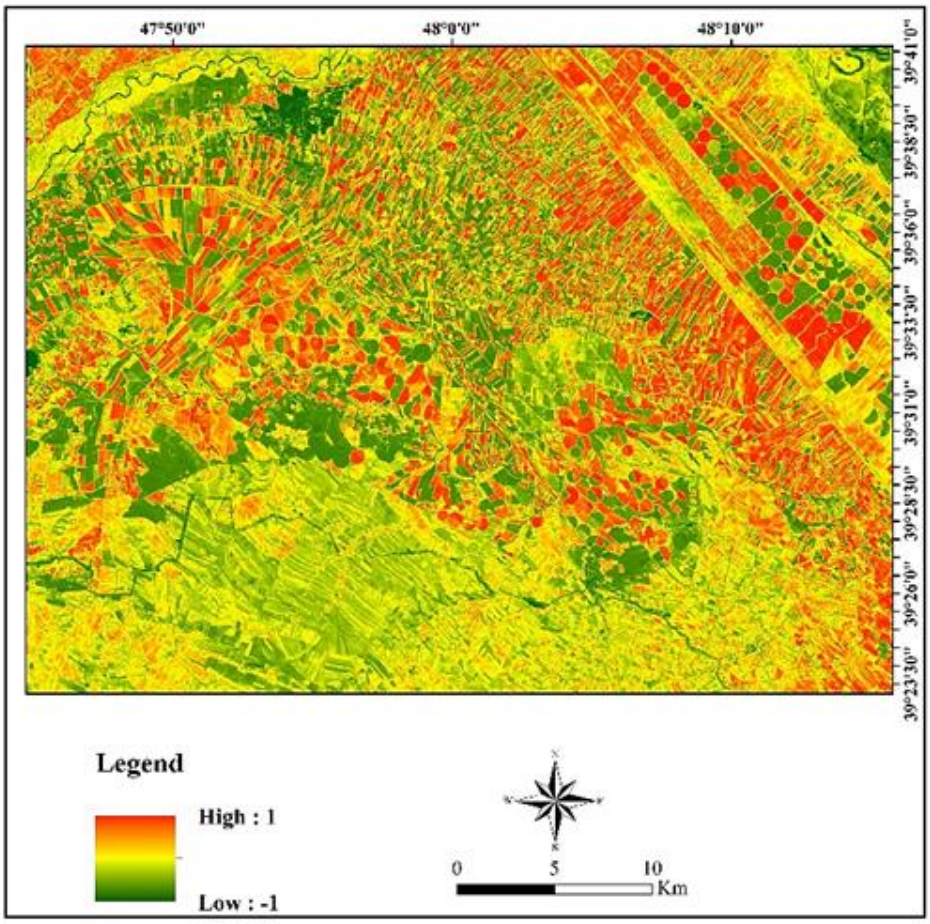

Figure 2. Normalized difference vegetation index (NDVI).

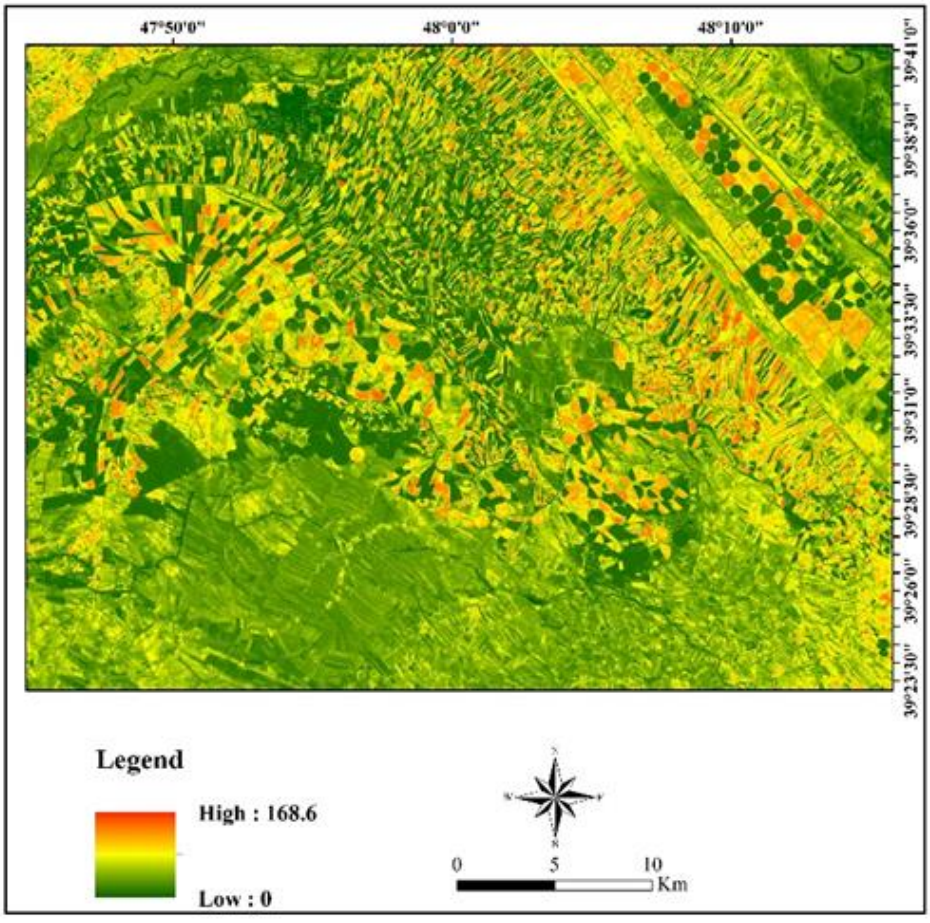

Figure 3. Leaf area index (LAI).

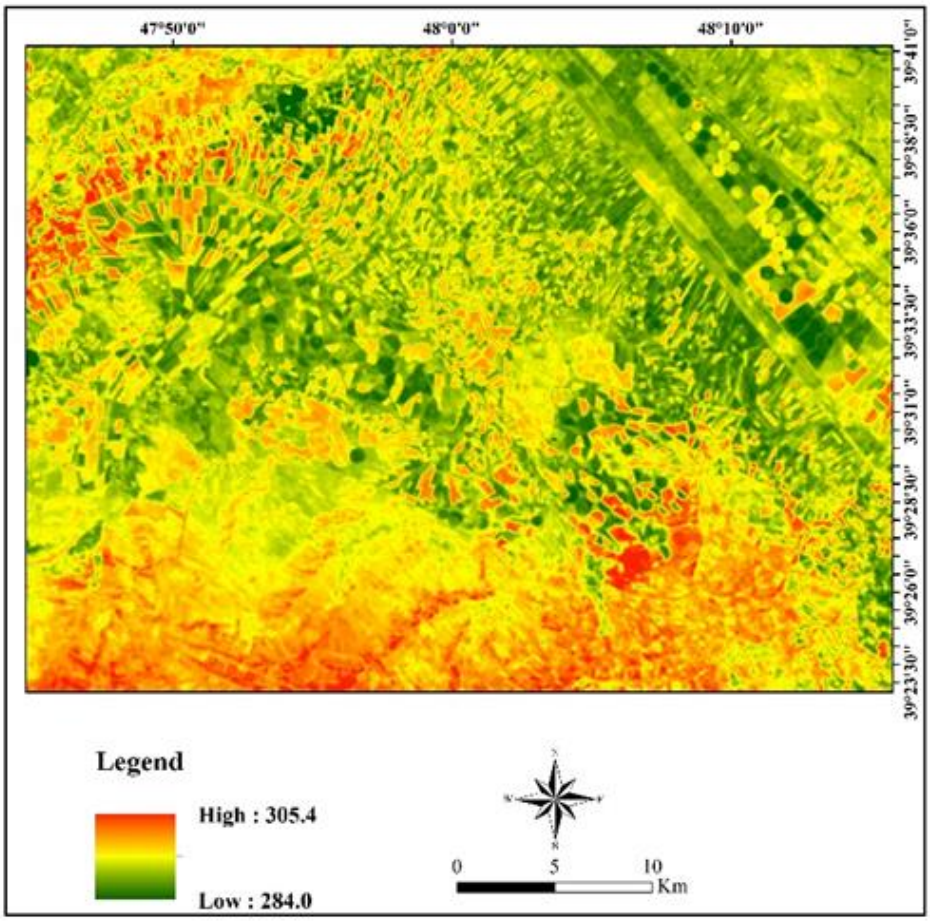

Figure 4. Land surface temperature.

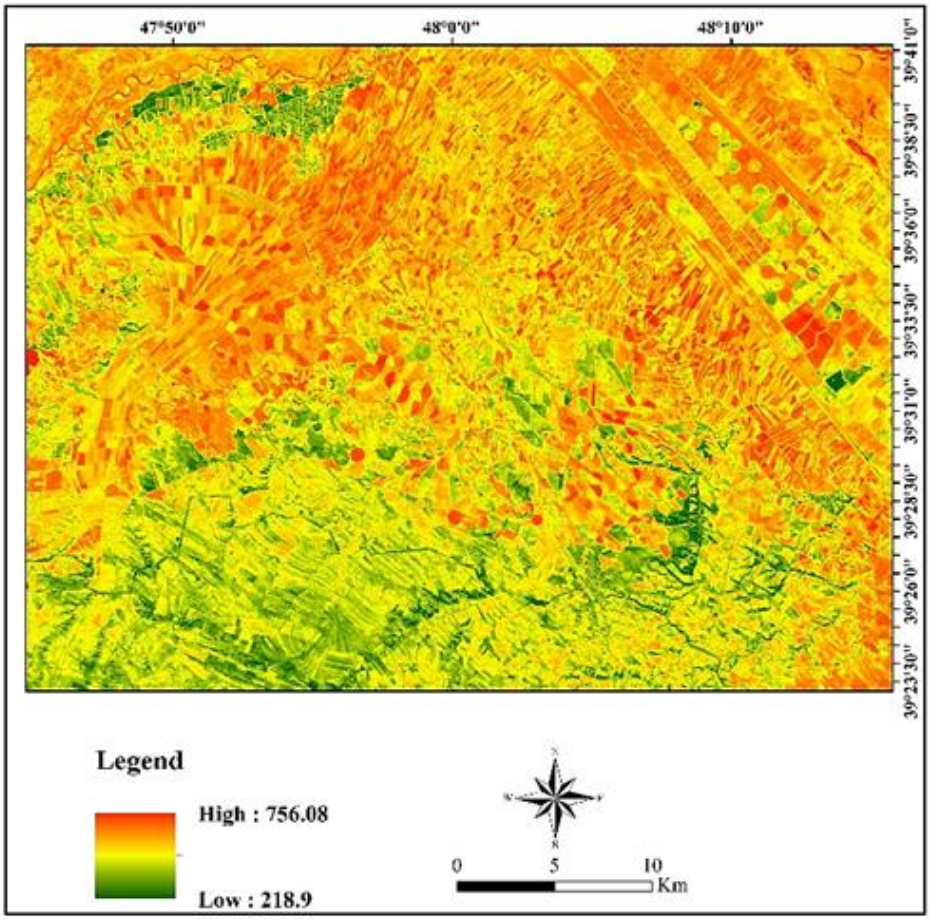

Figure 5. Net radiation (Rn).

The values of these emissivities are calculated using empirical Equation 17 and 18.

$$\text{For LAI} < 3: \varepsilon NB = 0.97 + 0.0033 \times LAI \quad (17)$$

$$\text{For LAI} \geq 3: \varepsilon_0 = 0.95 + 0.01 \times LAI \quad (18)$$

If LAI ≥ 3, the values of both emissivities are set to 0.98.

For water with α < 0.47 and NDVI < 0, and for snow with α > 0.47 and NDVI < 0, the values of both emissivities are set to 0.985 for ε_0 and 0.99 for εNB.

After calculating the required parameters, the net surface radiation (Rn) is computed as the final output in the SEBAL model (Figure 5).

2.3.1.9. Soil heat flux (G)

Soil heat flux is the amount of heat stored in the soil and vegetation cover on the Earth's surface due to molecular conduction processes. In the SEBAL model, the ratio of G/Rn is calculated using an empirical equation (Equation 19) presented by Allen (2000). In Equation 19, the temperature is in degrees Celsius (Figure 6).

$$G/Rn = (Ts / \alpha) * (0.0032\alpha + 0.007\alpha^2) * (1 - 0.98 * NDVI^4) \quad (19)$$

For clear and deep water and for snow, the ratio is set to 0.5. The values of this ratio for other land cover types are provided in Table 3.

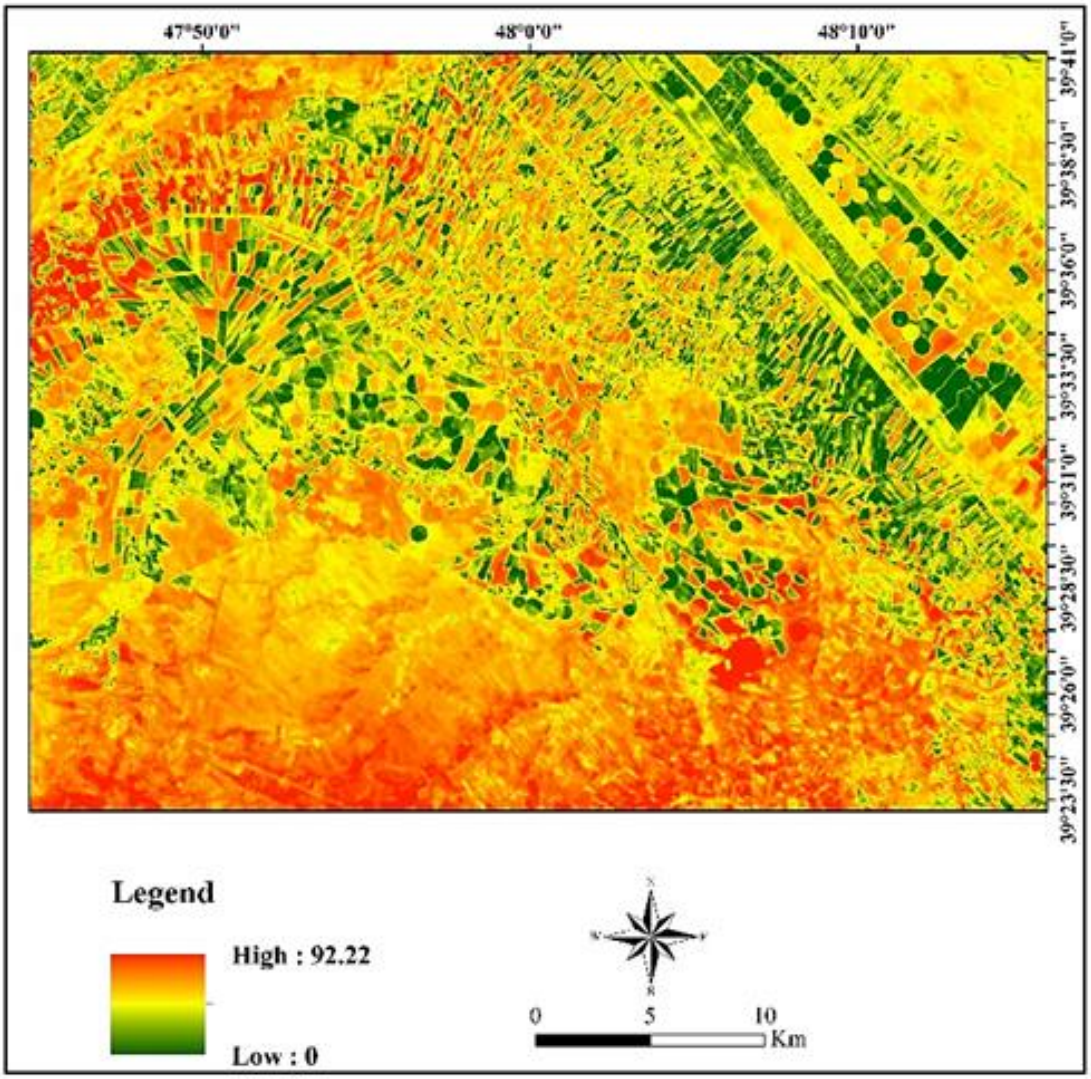

Figure 6. Soil Heat Flux (G).

Table 3. Values of G/Rn for some land cover types.

Surface type	G/Rn
Deep, Clear water	0.5
Snow	0.5
Desert	0.2 – 0.4
Agriculture	0.05 – 0.15
Bare Soil	0.2 – 0.4
Full Cover Alfalfa	0.04
Rock	0.2 – 0.6

2.3.1.10. Sensible heat flux (H)

Sensible heat flux represents the amount of heat loss from the surface to the air through processes of convection and molecular conduction due to temperature differences. Sensible heat flux is calculated using Equation (20) for heat transfer (Figure 7).

$$H = (\rho \times Cp \times dT) / rah \quad (20)$$

In Equation (20), ρ is the air density (kg/m^3), Cp is the specific heat of air (1004 J/kg/K), dT is the temperature difference (T1-T2) between two heights (Z1 and Z2), and rah is the aerodynamic resistance for heat transfer (s/m).

Initially, using data from synoptic weather stations, the wind speed at a distance of 200 meters above the ground (U 200) is calculated. Then, the friction velocity (U*) is estimated for each separate pixel. Finally, the aerodynamic resistance parameter (rah) is calculated for each pixel. After determining the aerodynamic resistance and air density, the coldest and warmest pixels are selected, and based on those, H_{cold} and H_{hot} are calculated. Subsequently, dt_{cold} and dt_{hot} are determined, leading to the final calculation of dt_{total}.

After obtaining the initial H, the aerodynamic resistance is corrected, and the sensible heat flux is recalculated. This cycle continues until the average values of aerodynamic resistances converge. In this study, the convergence of rah values were achieved after repeating this cycle five times (Figure 8).

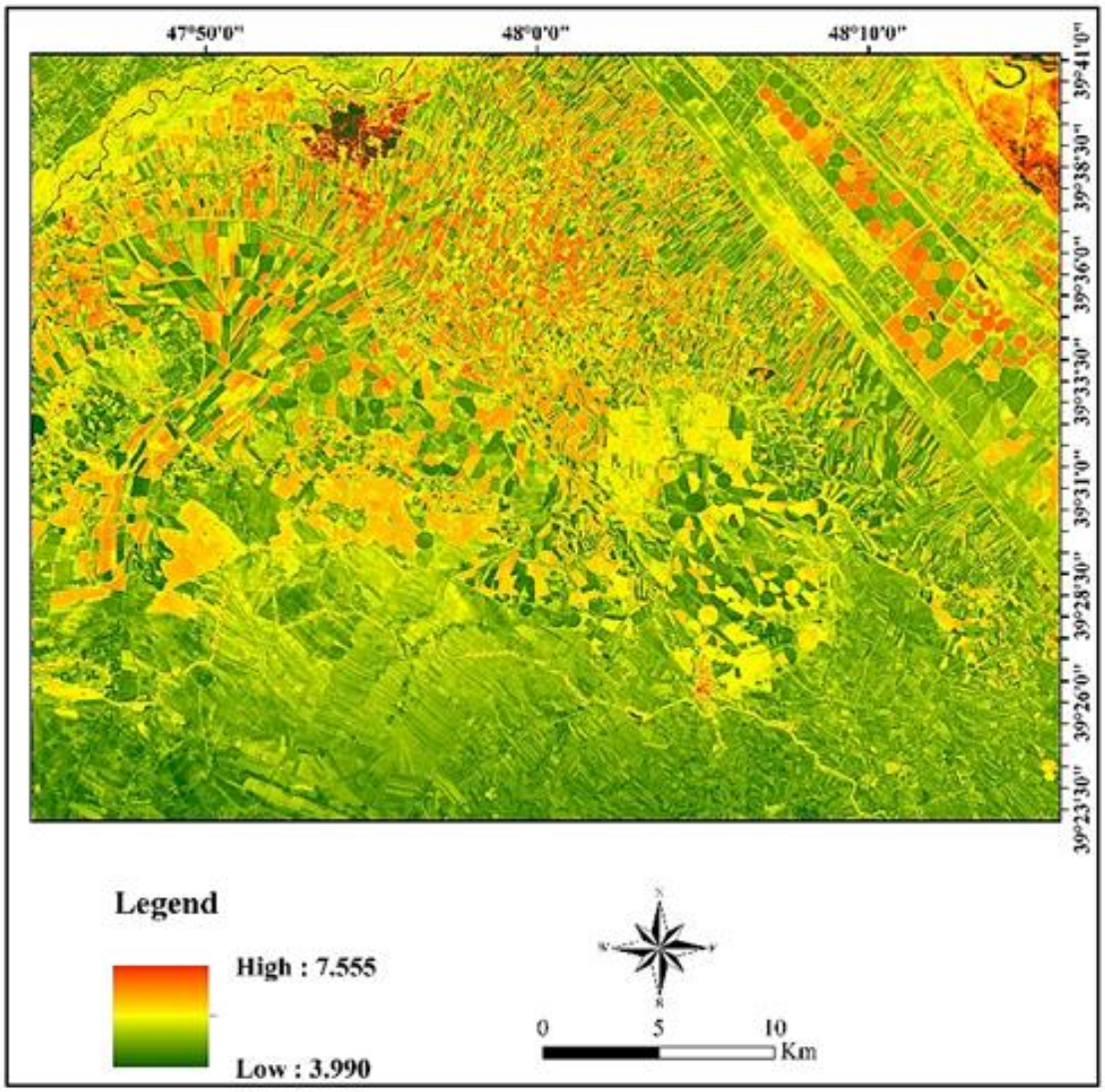

Figure 7. Corrected aerodynamic resistance.

2.3.1.11. Aerodynamic resistance to heat transport (rah)

Aerodynamic resistance is calculated using Equation (21).

$$rah = ln\ (Z2 / Z1) / (U^* \times K) \quad (21)$$

Z2: 2 meters (height above the surface)
Z1: 1/0 meters (reference height, typically at the surface)
U*: Friction velocity
K: Karman constant (0.41)

Parameters $u*$, Z0m, and u200were calculated using Equations (22, 23, and 24), respectively.

$$u* = \frac{kux}{ln\frac{zx}{zom}} \quad (22)$$

$$Z0m = 0.018*LAI \quad (23)$$

$$u200 = \mu * \frac{\ln\left(\frac{200}{zom}\right)}{k} \quad (24)$$

K: Karman constant (0.41)
Ux: Wind speed at height x
ZX: Height x
Z0m: Momentum roughness length (in meters)

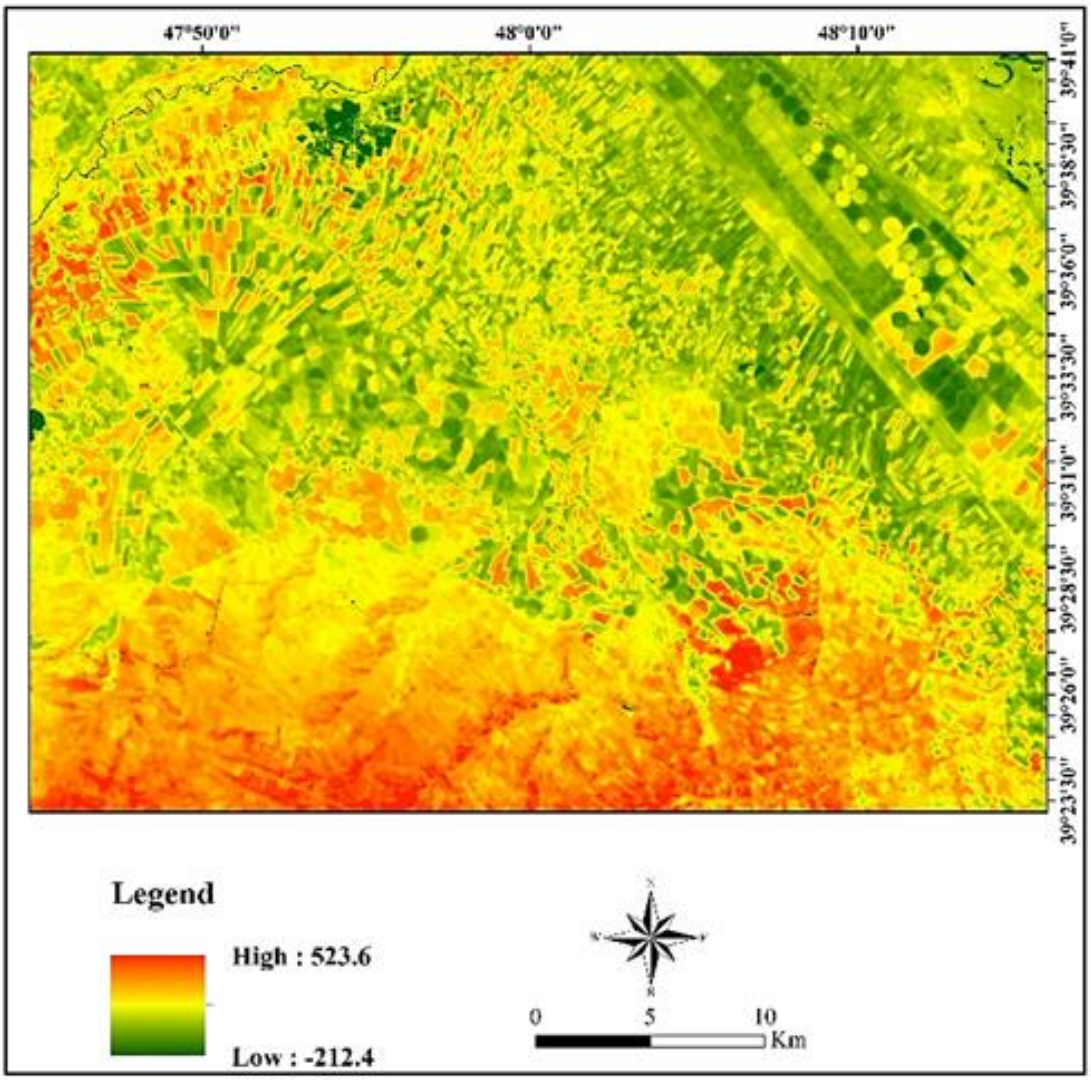

Figure 8. Sensible heat flux (H).

2.3.1.2. Cold and warm pixels

Sabal uses two reference pixels to determine the boundary conditions in the energy balance equation, which are called cold and warm pixels. Cold pixels are selected from fully irrigated fields and are free from moisture stress, appearing green and vibrant within the study area. In these pixels, the surface temperature and near-surface air temperature are assumed to be equal. Warm pixels are chosen from drylands with no vegetation cover [13] To select these two pixels, a complete understanding of the study area, familiarity with the spectral behavior of phenomena, and proficiency in interpreting images are necessary. The accuracy of calculating evapotranspiration in Sabal relies on the precise selection of these two reference pixels."

2.3.1.2.1. Calculation of H_{cold} and H_{hot}

H_{cold} and H_{hot} are calculated using Equation 25 and 26 respectively.

$$H_{cold} = Rn - G - \lambda ETr \quad (25)$$

λ: Latent heat of evaporation

ETr: Reference evapotranspiration for the cold pixel

In Equation (26), the reference evapotranspiration for the reservoir pixel is calculated using the FAO Penman-Monteith method and estimated to be 1743.0.

$$H_{hot} = Rn - G \quad (26)$$

The value of H_{hot} for the selected warm pixel is estimated to be 262.499. It is important to note that the value of H_{hot} should not be less than the value of H_{cold}.

2.3.1.2.2. Calculation of "dt_{cold}" and "dt_{hot}"

In the context of the original Equations 27 and 28, "dt_{cold}" and "dt_{hot}" are likely terms used in a specific scientific or engineering domain to represent temperature differences or changes. Without further context or specific information about the equations, it's challenging to provide a more precise translation. If you can provide more details or the full equations, I would be glad to assist further.

$$dTcold = Hcold \times rah / (\rho \times Cp) \quad (27)$$

$$dThot = Hhot \times rah\_ / (\rho \times Cp) \quad (28)$$

2.3.1.2.3. Modification of aerodynamic resistance

In order to correct the aerodynamic resistance, the length of the Monin-Obukhuv length (L) needs to be calculated (Equation 29). If the value of L is negative, it indicates atmospheric instability, and if L is zero or positive, it signifies atmospheric stability.

$$L= -(\rho C_p \mu^{*3} T_S)/kgH \quad (29)$$

ρ: Air density (kg/m^3)
Cp: Specific heat of air (1004 J/kg/K)
U*: Friction velocity
Ts: Surface temperature
K: 41/0
g: 81/9
H: Sensible heat flux

In order to converge the aerodynamic resistance, the correction cycle was repeated 5 times. which is shown in Figure 9.

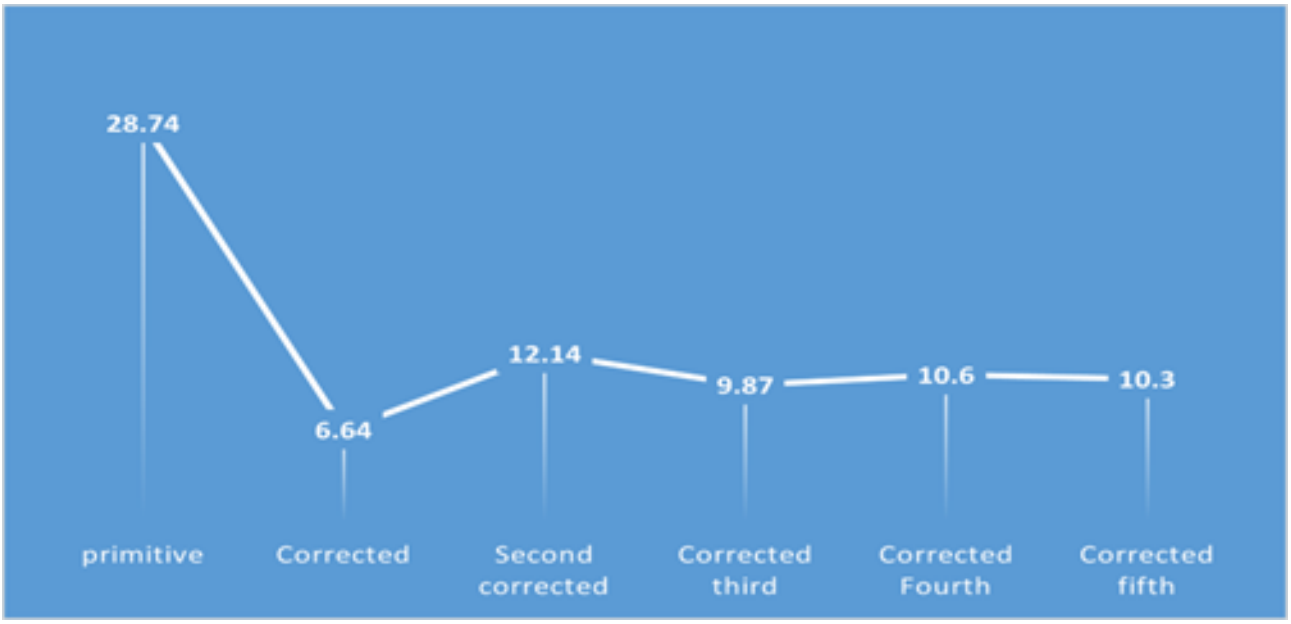

Figure 9. Aerodynamic resistance correction process

2.4. Instantaneous and daily evapotranspiration (ET)

To calculate instantaneous and daily evapotranspiration (ET) after estimating the parameters Rn, G, and H, you can use the Equation 30:

$$ET\lambda = Rn - G - H \quad (30)$$

ETλ: Latent heat flux (J/m^2/s)
Rn: Net radiation (J/m^2/s)
G: Soil heat flux (J/m^2/s)
H: Sensible heat flux (J/m^2/s)

The instantaneous evapotranspiration (ETinst) can be calculated as (Equation 31):

$$ETinst = 3600 * (\lambda ET / \lambda) \quad (31)$$

ETinst: Instantaneous evapotranspiration (mm/hr)
λ: Latent heat of evaporation of water or the amount of heat needed to evaporate one kilogram of water (J/kg)
3600: Conversion factor from seconds to hours

The value of λET can be obtained from Equation (32). To calculate the daily evapotranspiration (ET24), which has more practical significance compared to instantaneous evapotranspiration, the following steps are taken:

$$ETrF = ETinst / ETr \quad (32)$$

ETrF: Fraction of daily reference evapotranspiration
ETinst: Instantaneous evapotranspiration (mm/hr)
ETr: Reference evapotranspiration, which is the average 24-hour evapotranspiration

Daily evapotranspiration was calculated using Equation 33.

$$ET24 = ETrF * ETr\text{-}24 \quad (33)$$

ET24: Daily evapotranspiration (mm/day)
ETrF: Fraction of daily reference evapotranspiration (dimensionless)
ETr-24: Total sum of reference evapotranspiration over 24 hours (mm/day)

ETr-24 is obtained by summing up the hourly values of ETr during the day of interest, which can be derived from satellite data. ETr-24 is estimated using CROPWAT software with synoptic data at 5.4 mm per day for the study area.

After calculating Rn, G, and H, the latent heat flux (ETλ) is determined, and then the instantaneous actual evapotranspiration (ETinst) is estimated (Figure 10). Finally, the daily actual evapotranspiration is calculated in millimeters per day (Figure 11).

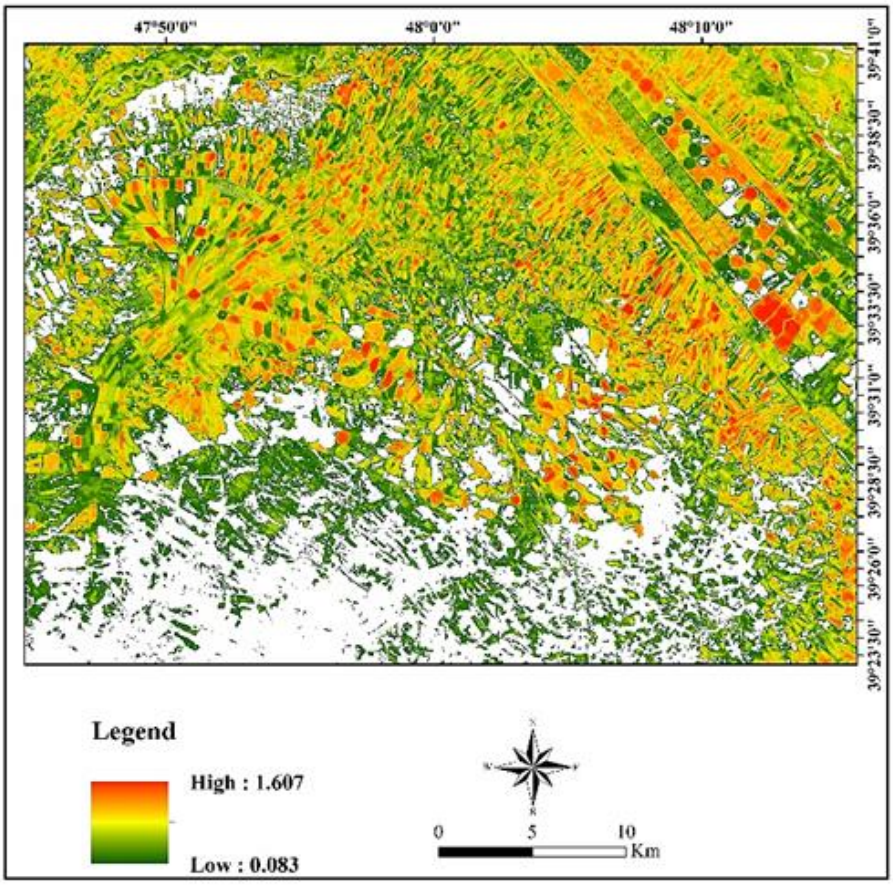

Figure 10. instantaneous actual evapotranspiration (ETinst) (mm/hr) (SEBAL).

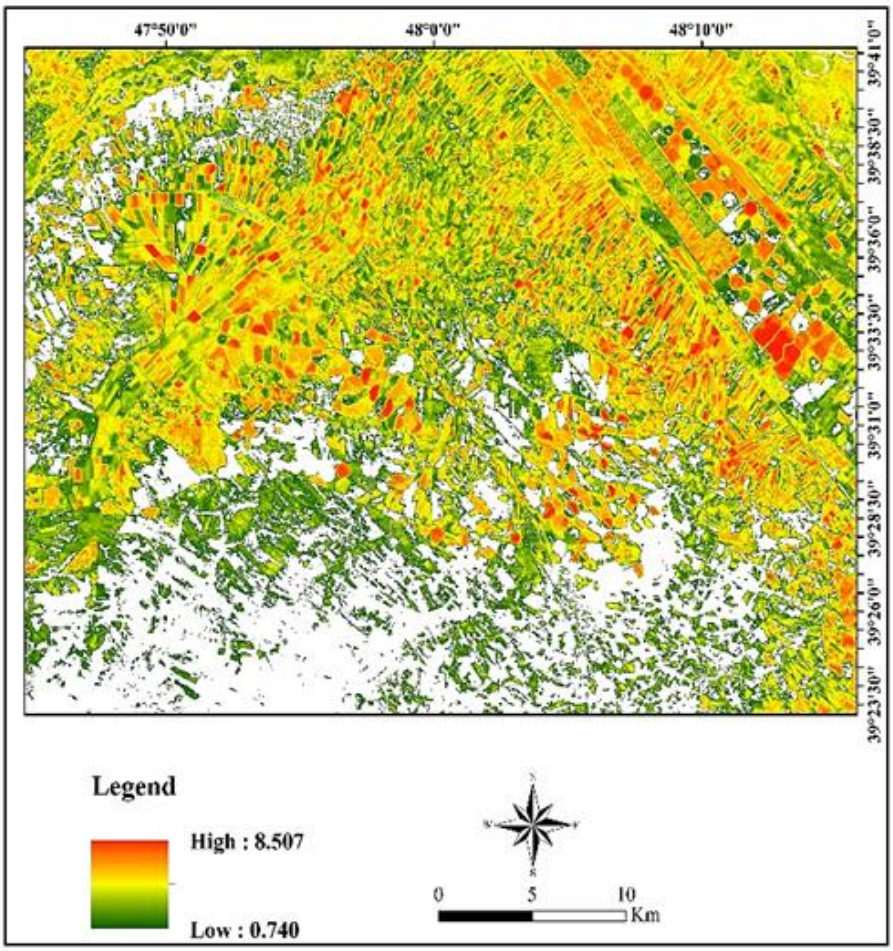

Figure 11. Daily actual evapotranspiration (SEBAL).

2.3.2. The SEBS method

SEBS is based on the Crop Water Stress Index (CWSI; [14]), idea in which the surface meteorological scaling of CWSI is replaced with planetary boundary layer (PBL) scaling. It uses the contrast between wet and dry areas appearing within a remotely sensed scene to derive ET from the relative evaporative fraction.

The basis of this method is to use the energy balance equation and calculate the latent heat flux as the residual of this equation for each pixel. This approach follows similar theoretical principles as the SEBAL algorithm.

The required input data include layers generated from satellite images and data obtained from weather stations. The output of the SEBS algorithm, unlike the SEBAL algorithm, provides daily actual evapotranspiration.

2.3.2.1. Evapotranspiration

The surface energy balance is commonly written as (Equation 34):

$$Rn=G0+H+\lambda E \tag{34}$$

where Rn is the net radiation flux, G0 is the soil surface heat flux, H is the sensible heat flux, and λE is the latent heat flux. The unit of energy balance terms is watts per square meter.

To estimate the evaporative fraction, SEBS makes use of energy balance at limiting cases at dry limit and wet limit, such that the relative evaporation (ratio of the actual evaporation to the evaporation at wet limit) can be derived as (Equation 35):

$$\Lambda r = 1 - \frac{H - Hwet}{Hdry - Hwet} \tag{35}$$

where the H wet is sensible heat flux at the wet limit and H dry sensible heat flux at the dry limit. The estimations of H wet and H dry were detailed by Su [15]. The evaporative fraction (ratio of latent heat flux to available energy) is estimated by (Equation 36 and 37):

$$Rn-G \tag{36}$$

$$\Lambda = \frac{\lambda E}{Rn - G} = \frac{\Lambda r.\lambda E\ wet}{Rn - G} \tag{37}$$

where λE wet is the latent heat flux at the wet limit (i.e., the evaporation is only limited by the available energy under the given surface and atmospheric conditions). The latent heat flux (λE) can then be calculated by (Equation 38):

$$\lambda E=\Lambda(Rn-G0) \tag{38}$$

Finally, the daily actual ET can be written (Equation 39):

$$ET= 8.64 \times 107 \times \Lambda 24 \times \frac{Rn-G0}{\lambda \rho w} \tag{39}$$

where ρw is the density of water (1, 000 kgm^{-3}) and Rn is the average daily net radiation in this equation. Moreover, the soil heat flux G0 for 24 h is normally assumed negligible (G average).

2.3.2.2. Daily actual evapotranspiration

The results of the daily evapotranspiration calculated by the SEBS algorithm are presented in Figure 12.

3. Results

The results obtained from the SEBAL and SEBS algorithms indicate that the SEBAL algorithm exhibits a broader range of actual evapotranspiration values (0.74 to 5.8 millimeters) compared to the SEBS algorithm (1.25 to 8.85 millimeters), demonstrating its greater capability in distinguishing areas with different evapotranspiration rates. On the other hand, the implementation of the SEBAL algorithm is more complex and time-consuming compared to SEBS. The results showed that both algorithms have relatively high capabilities in calculating instantaneous evapotranspiration using spectral data. Estimating plant water consumption on a pixel-by-pixel (spatial) basis is a unique advantage of spectral methods, as other empirical methods provide a single value estimation for all farms and different varieties of a crop. Generally, satellite data has the potential to estimate evapotranspiration for different plant species. Additionally, due to the pixel-based nature of satellite data, it allows for estimating surface properties such as temperature, emissivity, and actual evapotranspiration within a specific region instead of point-based estimation (at a stationary location). This capability is perhaps one of the most important characteristics of satellite data, as it enables the investigation and analysis of spatially distributed environmental characteristics. Therefore, it is recommended that when investigating spatial and temporal changes in environmental variables, the use of raster data, or satellite data, is highly advantageous as it can significantly aid in such investigations with minimal time and cost. The valuable results obtained from such analyses can be crucial for resource management. Additionally, considering the scarcity and inadequate distribution of weather stations and the subsequent unavailability of synoptic data in the country, employing methods based on digital data is highly suitable.

4. Discussion

The study aimed to estimate actual evapotranspiration using the SEBAL and SEBS algorithms and spectral data from the OLI and TIRS sensors of the Landsat 8 satellite in the Mughan plain of Ardabil province. The results of the analysis revealed valuable insights into the performance of these algorithms and their applicability in the specific study area.

Firstly, the comparison between the SEBAL and SEBS algorithms demonstrated distinct differences in their estimated values of actual evapotranspiration. The SEBAL algorithm showed a wider range of values, indicating its ability to discern variations in

evapotranspiration rates across different areas in the Mughan plain. On the other hand, the SEBS algorithm provided a more limited range of values, suggesting a somewhat less nuanced representation of the spatial distribution of evapotranspiration.

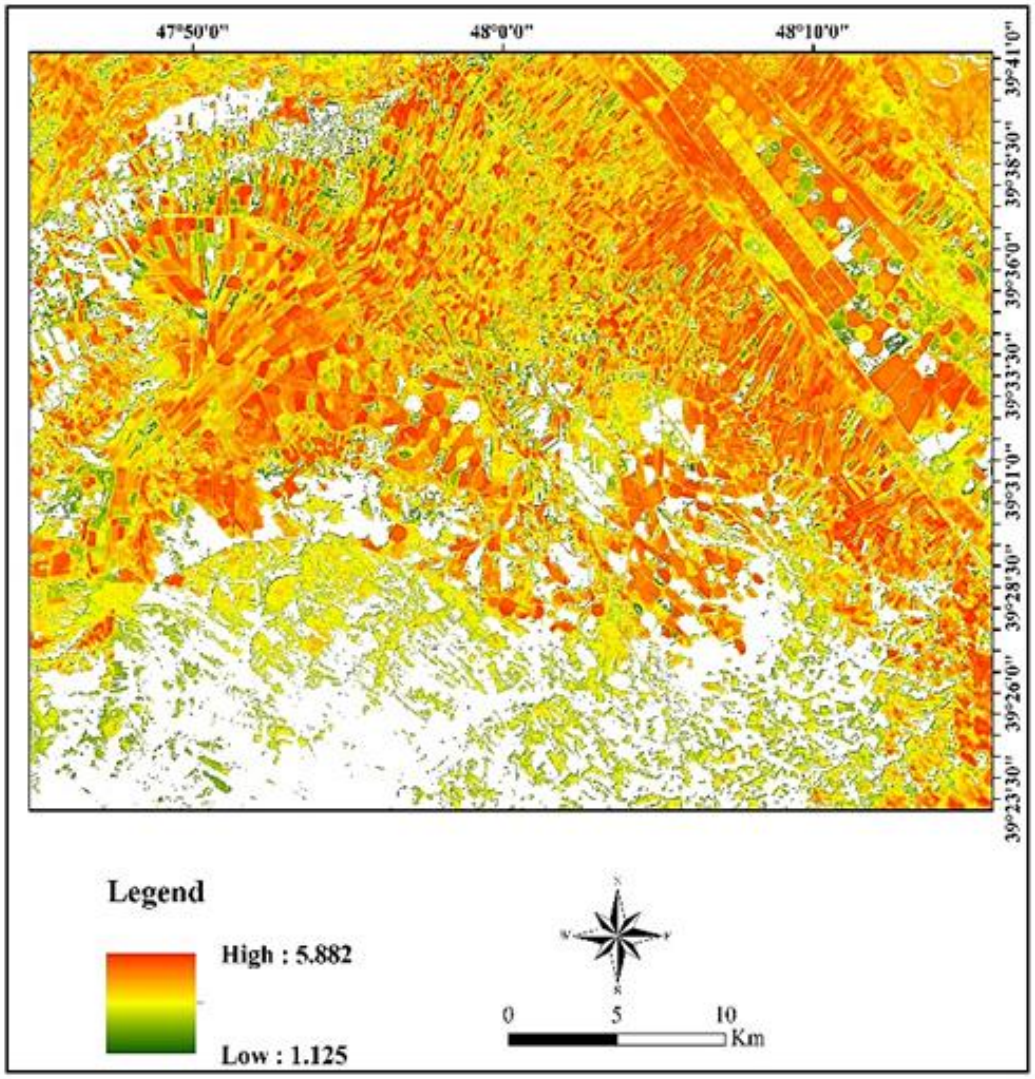

Figure 12. Daily actual evapotranspiration (SEBS).

Secondly, while the SEBAL algorithm exhibited superior capabilities in distinguishing areas with different evapotranspiration rates, it also presented challenges in terms of computational complexity and time consumption. This issue needs to be considered when implementing SEBAL for large-scale or time-sensitive applications.

Furthermore, the utilization of spectral data from the OLI and TIRS sensors of Landsat 8 enabled a pixel-based approach to estimate evapotranspiration. This pixel-level estimation offers a significant advantage over point-based methods since it allows for a more comprehensive analysis of surface properties, such as temperature, emissivity, and actual evapotranspiration, within specific regions. This spatially distributed information provides valuable insights into the environmental characteristics of the study area.

Overall, the results indicated that both SEBAL and SEBS algorithms have relatively high capabilities in estimating instantaneous evapotranspiration using spectral data. This finding highlights the potential of satellite data for accurately estimating evapotranspiration for various plant species. However, it is essential to consider the trade-off between the finer spatial resolution and computational complexity when choosing the most suitable algorithm for a particular study.

The results of this research, in comparison with the findings of previous studies such as the calculation of actual evapotranspiration using the SEBAL algorithm by Asadi and Valizadeh Kamran [5], Wei et al [7], and Ma et al [8], as well as the estimation of actual evapotranspiration using the SEBS algorithm by Yang and colleagues [6] and Matinfar & Soorghali [4], are consistent.

5. Conclusion and suggestions

In conclusion, the study successfully demonstrated the application of SEBAL and SEBS algorithms in estimating actual evapotranspiration in the Mughan plain. The findings contribute valuable information to water resource management, agricultural planning, and

environmental studies in the region. Additionally, the use of spectral data from satellite sensors opens up possibilities for further investigations into the spatial distribution of environmental variables, enhancing our understanding of the local climate and water balance. the application of the SEBAL and SEBS algorithms, along with spectral data from the OLI and TIRS sensors of the Landsat 8 satellite, proved to be a successful approach in estimating actual evapotranspiration in the Mughan plain of Ardabil province. The study provided valuable insights into the spatial distribution of evapotranspiration rates, shedding light on the water balance dynamics and environmental characteristics of the region.

The findings of this research lead to several key conclusions and offer valuable suggestions for future studies:

Algorithm Performance: Both SEBAL and SEBS algorithms demonstrated the capability to estimate actual evapotranspiration using satellite data. However, further comparative analysis and validation against ground-based measurements are recommended to identify the strengths and weaknesses of each algorithm for specific study areas and environmental conditions. Spatial and Temporal Variability: The observed wide range of evapotranspiration values highlights the spatial variability in water use and transpiration rates across the Mughan plain. It is essential to consider this variability in water resource management and agricultural planning to optimize irrigation practices and ensure sustainable water use.

Data Integration and Validation: Integrating data from multiple satellite sensors and ground-based measurements can enhance the accuracy of evapotranspiration estimates. Validation of remote sensing-derived results through field measurements is critical to ensuring reliable and precise evapotranspiration calculations. Long-Term Monitoring: Continuous monitoring of evapotranspiration over time can provide valuable insights into climate trends and changes in water availability. Establishing long-term monitoring networks and using historical satellite data can contribute to a better understanding of the region's hydrological dynamics.

Application in Water Resource Management: The estimated evapotranspiration data can be instrumental in water resource management and decision-making processes. Utilizing this information can aid in the sustainable use of water resources and improve irrigation practices in the Mughan plain and other similar regions. Climate Change Implications: Considering the potential impact of climate change on evapotranspiration patterns is essential for anticipating future water availability and planning for adaptation measures. Future studies should explore the correlation between evapotranspiration and climate change indicators.

Capacity Building: Promoting capacity building initiatives among researchers and practitioners in remote sensing and hydrological modeling can enhance the application of these techniques in water resource management and environmental studies. Data Accessibility: Ensuring open access to remote sensing data and making relevant datasets publicly available can foster collaboration and enable more researchers to contribute to advancing the understanding of evapotranspiration dynamics.

In conclusion, this study lays the groundwork for further investigations into evapotranspiration dynamics in the Mughan plain and serves as a valuable resource for water resource management and agricultural planning. The implementation of the suggested improvements can lead to more accurate and comprehensive assessments of evapotranspiration in the region and contribute to sustainable water management strategies.

Author contributions

Khalil Valizadeh Kamran: Conceptualization, Methodology, Data collecting. **Mahmoud Sourghali:** Analysis, Visualization, Writing-Reviewing. **Samaneh Bagheri:** Investigation, Editing, Writing-Reviewing

Conflicts of interest

The authors declare no conflicts of interest.

References

1. Erdoğan, A., Görken, M., Kabadayı, A., & Temizel, S. (2022). Evaluation of green areas with remote sensing and GIS: A case study of Yozgat city center. Advanced Remote Sensing, 2(2), 58–65.
2. Kotan, B., Tatmaz, A., Kılıç, S., & Erener, A. (2021). LST change for 16-year period for different land use classes. Advanced Remote Sensing, 1(1), 38-45.
3. Çelik, M. Ö., & Yakar, M. (2023). Arazi kullanımı ve arazi örtüsü değişikliklerinin uzaktan algılama ve cbs yöntemi ile izlenmesi: Mersin, Türkiye örneği. Türkiye Coğrafi Bilgi Sistemleri Dergisi, 5(1), 43-51. https://doi.org/10.56130/tucbis.1300704
4. Matinfar, H. R., & Soorghali, M. (2014). Estimate evapotranspiration (ET) using SEBS model based on Landsat 5 (TM) thermal data and GIS. Indian Journal of Fundamental and Applied Life Sciences, 4(3), 30-34.
5. Asadi, M., & Kamran, K. V. (2022). Comparison of SEBAL, METRIC, and ALARM algorithms for estimating actual evapotranspiration of wheat crop. Theoretical and Applied Climatology, 149(1), 327-337. https://doi.org/10.1007/s00704-022-04026-3
6. Yang, Y., Sun, H., Xue, J., Liu, Y., Liu, L., Yan, D., & Gui, D. (2021). Estimating evapotranspiration by coupling Bayesian model averaging methods with machine learning algorithms. Environmental Monitoring and Assessment, 193, 1-15. https://doi.org/10.1007/s10661-021-08934-1
7. Wei, J., Cui, Y., & Luo, Y. (2023). Rice growth period detection and paddy field evapotranspiration estimation based on an improved SEBAL model: Considering the applicable conditions of the advection equation. Agricultural Water Management, 278, 108141. https://doi.org/10.1016/j.agwat.2023.108141

8. Ma, Y., Sun, S., Li, C., Zhao, J., Li, Z., & Jia, C. (2023). Estimation of regional actual evapotranspiration based on the improved SEBAL model. Journal of Hydrology, 619, 129283. https://doi.org/10.1016/j.jhydrol.2023.129283
9. Orhan, O., Dadaser-Celik, F., & Ekercin, S. (2019). Investigating land surface temperature changes using Landsat-5 data and real-time infrared thermometer measurements at Konya closed basin in Turkey. International Journal of Engineering and Geosciences, 4(1), 16-27. https://doi.org/10.26833/ijeg.417151
10. Waters, R., Allen, R., Tasumi, M., Trezza, R., & Bastiaanssen, W. (2002). Surface energy balance algorithms for land. Advanced Training and User's Manual.
11. Jensen, M. E., Burman, R. D., & Allen, R. G. (1990). Evapotranspiration and irrigation water requirements: a manual. ASCE manuals and reports on engineering practice (USA), 70.
12. Bastiaanssen, W. G. M. (2000). SEBAL-based sensible and latent heat fluxes in the irrigated Gediz Basin, Turkey. Journal of hydrology, 229(1-2), 87-100. https://doi.org/10.1016/S0022-1694(99)00202-4
13. Jackson, R. D., Idso, S. B., Reginato, R. J., & Pinter Jr, P. J. (1981). Canopy temperature as a crop water stress indicator. Water Resources Research, 17(4), 1133-1138. https://doi.org/10.1029/WR017i004p01133
14. Jackson, R. D., Idso, S. B., Reginato, R. J., & Pinter Jr, P. J. (1981). Canopy temperature as a crop water stress indicator. Water resources research, 17(4), 1133-1138. https://doi.org/10.1029/WR017i004p01133
15. Su, Z. (2002). The Surface Energy Balance System (SEBS) for estimation of turbulent heat fluxes. Hydrology and Earth System Sciences, 6(1), 85-100. https://doi.org/10.5194/hess-6-85-2002